

Evolutionary Kuramoto dynamics unravels origins of chimera states in neural populations

Thomas Zdyrski¹, Scott Pauls¹, and Feng Fu^{1,2}

¹Department of Mathematics, Dartmouth College, Hanover, NH 03755

²Department of Biomedical Data Science, Geisel School of Medicine at
Dartmouth, Lebanon, NH 03756 .

Abstract

Neural synchronization is central to cognition^{1,2}. However, incomplete synchronization often produces chimera states^{3,4}, where coherent and incoherent dynamics coexist. While previous studies⁵ have explored such patterns using networks of coupled oscillators, it remains unclear why neurons commit to communication or how chimera states persist. Here, we investigate the coevolution of neuronal phases and communication strategies on directed, weighted networks, where interaction payoffs depend on phase alignment⁶ and may be asymmetric due to unilateral communication. We find that both connection weights and directionality influence the stability of communicative strategies—and, consequently, full synchronization—as well as the strategic nature of neuronal interactions. Applying our framework to the *C. elegans* connectome⁷⁻⁹, we show that emergent payoff structures, such as the snowdrift game, underpin the formation of chimera states. Our computational results demonstrate a promising neurogame-theoretic perspective, leveraging evolutionary graph theory to shed light on mechanisms of neuronal coordination beyond classical synchronization models.

001
002
003
004
005
006
007
008
009
010
011
012
013
014
015
016
017
018
019
020
021
022
023
024
025
026
027
028
029
030
031
032
033
034
035
036
037
038
039
040
041
042
043
044
045
046

047 1 Introduction

048

049 Evolutionary game theory (EGT) is the application of game theory to evolving
050 populations of individuals with behavioral strategies. This tool is useful for studying how
051 local interaction rules yield large-scale patterns such as cooperation¹⁰ and has found use
052 in fields including international politics, ecology, and protein folding¹¹. Studies^{6,12,13}
053 have even applied EGT to non-reproducing neurons by viewing neuron plasticity as
054 an evolutionary process where firing patterns change and are “learned” over time.
055 Evolutionary *graph* theory places evolutionary games on graphs to investigate the role of
056 structure in population evolution. Prior studies have found that structure qualitatively
057 changes game evolution. For instance, cooperation is enhanced by small-degree nodes¹⁴
058 or unidirectional edges¹⁵ and suppressed by weighted edges¹⁶. Thus, the study of
059 evolving, structured populations should account for the effects of incompleteness,
060 directedness, and weightedness.

061 Kuramoto networks are groups of coupled oscillators where the coupling strength
062 depends sinusoidally on the oscillators’ phase difference. These networks are popular
063 models for neuron behaviour^{17,18} because they exhibit tunable synchronization. Prior
064 studies¹³ have modelled interneuron communication with Kuramoto oscillators and
065 EGT using the prisoner’s dilemma game type. Other studies⁶ generalized this approach
066 to include dynamically changing game types by introducing an evolutionary Kuramoto
067 (EK) model to show how the relationship between communication benefit and cost
068 influences the emergence of synchronized communication or non-communication
069 regimes.

070 One intriguing aspect of neuron oscillations is the observation of chimera states³.
071 These states exhibit the simultaneous existence of coherent and disordered phases⁵.
072 Previous studies have proposed chimera states as a key component of human cognitive
073 organization², a facilitator of spiking and bursting phases¹, and an outcome of modular
074 organization², a facilitator of spiking and bursting phases¹, and an outcome of modular
075 organization², a facilitator of spiking and bursting phases¹, and an outcome of modular

076

077

078

079

080

081

082

083

084

085

086

087

088

089

090

091

092

networks⁴. Despite the observed importance of these chimera states, the factors that give rise to coherent/disordered coexistence remain incompletely characterized.

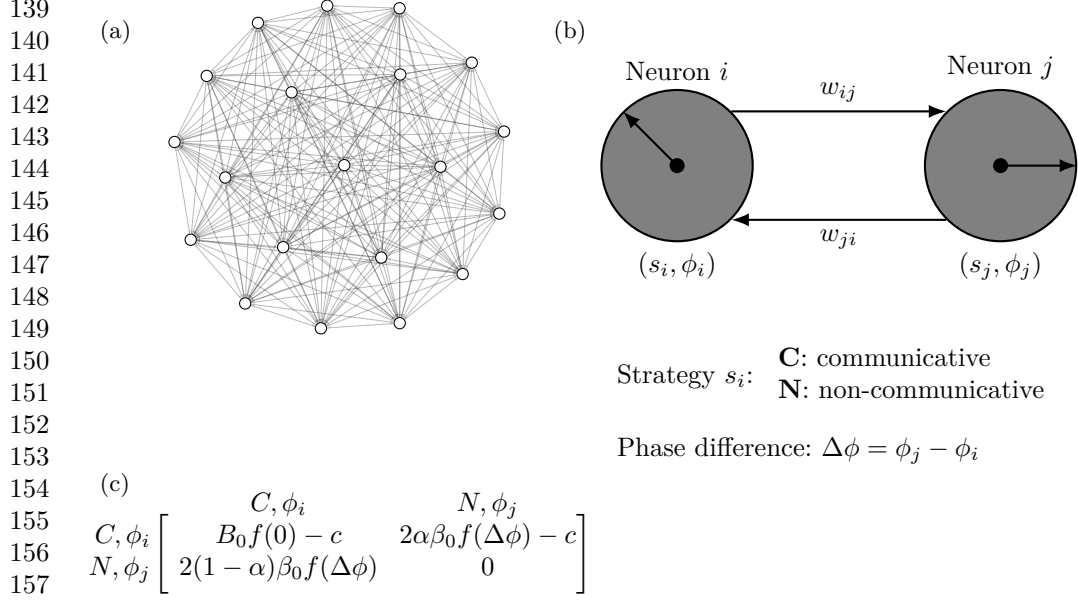
The nematode *Caenorhabditis elegans* (*C. elegans*) is a model organism in neuroscience due to its simple brain connectome⁷ of only 302 neurons. Despite their simplicity, models of the *C. elegans* brain still display a wide array of complex phenomena including topologically-central rich clubs crucial to motor neurons⁸, phenomenological connections to control theory⁹, and chimera states⁴.

In this paper, we introduce an asymmetric evolutionary Kuramoto model and analyze its chimera-like states on the *C. elegans* connectome. Our results connect individual neuron fitness and non-trivial brain topology to chimera-like brain states. Given current technological limitations with direct measurement of in-vivo neuron activity, frameworks like ours create testable hypotheses connected to the theory's assumptions. Our computational model represents a simple yet versatile framework to illuminate the influence of neural connectivity on chimera-like brain states beyond classical synchronization models.

2 Results

2.1 Model

We extend the EK model in two ways: placing the player network on a directed, weighted graph; and introducing a payoff asymmetry. First, we represent a well-mixed population as a complete graph in Fig. 1(a) with players represented by nodes and games by edges. We generalize this to directed graphs where game (edge) payoffs only flow to the head players (nodes). We can also represent bidirectional games with a pair of edges in both directions, as shown in Fig. 1(b). For reference, the *C. elegans* connectome has 38 self-loops, 669 bidirectional edge pairs, and 2,331 unpaired edges. Finally, we interpret the *C. elegans* chemical connectome's integer-valued edge weights as the number of connections between nodes, so these weights scale each payoff.



160 **Fig. 1| Evolutionary Kuramoto dynamics with weighted neural connectivity.**
161 (a) The graph of a well-mixed population with $N = 20$ players where each pair of
162 players is connected by a directed edge in each direction. (b) The connectivity between
163 two sample players, i and j , showing directed, weighted edges w_{ij} and w_{ji} . Each player
164 has a strategy (communicative C or non-communicative N) and phase $\phi = 2\pi k/m$
165 with $k \in 0, \dots, m - 1$ and m the number of phases. (c) The payoff matrix shows the
166 reward the row-player (C, ϕ_i) receives after playing a game with the column-player
167 (N, ϕ_j) assuming either player can switch strategy and phase to the other's.

168
169
170 We also generalize the payoff structure to incorporate an asymmetry between
171 communicators and non-communicators. We characterized each player (node) by
172 its strategy s_i —either communicative C or non-communicative N — and its phase
173 ϕ_i —taking one of $m = 20$ evenly-spaced values between 0 and 2π . When exactly one
174 partner is communicative, the asymmetry $\alpha \in [0, 1]$ biases the payoff toward (against)
175 the communicator when α is greater (less) than $1/2$, while $\alpha = 0.5$ reproduces the
176 symmetric case. Figure 1(c) shows the payoff matrix for these mixed CN or NC
177 interactions and includes the maximum joint benefit $B_0 = 0.15$, maximum mixed
178 benefit β_0 , cost c , and sinusoidal Kuramoto coupling $f(\Delta\phi) = [1 + \cos(\phi_j - \phi_i)]/2$.
179
180
181
182
183
184

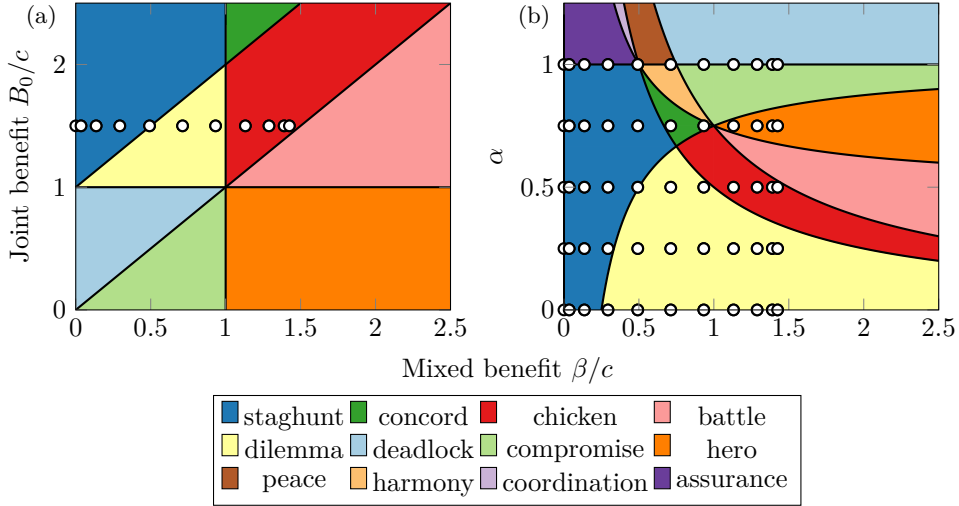


Fig. 2 | Payoff asymmetry enriches neural interactions well beyond the classic prisoner’s dilemma game type. Region plots illustrate the diverse range of game types that neural populations can engage in during evolutionary dynamics. Slices of the three-parameter mixed CN game-type phase diagram in the (a) β - B_0 plane ($\alpha = 0.5$) and (b) β - α plane ($B_0/c = 1.5$). For two players with phase difference $\Delta\phi$, the mixed benefit is $\beta = \beta_0[1 + \cos(\Delta\phi)]/2$. The legend displays the game type corresponding to each color. The white dots represent the $m = 20$ potential phase differences as well as the restriction (a) $B_0/c = 1.5$ or (b) $\alpha \in [0, 0.25, 0.5, 0.75, 1]$.

Unless otherwise specified, each simulation uses $m = 20$ phases, selection strength of $\delta = 0.2$, mutation rate of $\mu = 1 \times 10^{-4}$, cost c of 0.1, maximum joint benefit $B_0 = 0.15$, maximum mixed benefit β_0 of $0.95B_0$, and runs for 8×10^6 time steps (even if only a smaller time series subset is shown).

2.2 Parameter space

One of the key aspects of the EK model is that multiple 2×2 game types can emerge among the players during the population’s evolution. These game types¹⁹ include dilemma (*a.k.a.* “prisoner’s dilemma”), deadlock (“anti-prisoner’s dilemma”), chicken (“hawk-dove” or “snowdrift”), hero (“Bach or Stavinsky” with the lowest two payoffs swapped), harmony (game with strong incentive alignment), or concord (similar to harmony, weaker incentives). See Section 2 of the supplementary material for order

231 graphs depicting the payoff structure of each game type. While CC interactions are
 232 always double-cooperation games and NN interactions are always neutral games,
 233 mixed (CN or NC) games show a variety of game types, (Fig. 2). We can visualize
 234 these games by looking at two-dimensional slices of the three-dimension phase space
 235 characterized by α , $\beta := \beta_0 f(\Delta\phi)$, and B_0 . Fig. 2(a) shows a β - B_0 slice of phase space
 236 and generalizes figure 1 of a prior study⁶, while Fig. 2(b) shows a β - α slice. Each
 237 straight line of white dots represent permissible values of the $m = 20$ phases $\Delta\phi_i$
 238 across our simulations and highlight which regions of parameter space are accessible.
 239
 240
 241
 242
 243
 244

245 2.3 Complete graphs

246
 247 First, we will explore the influence of the newly introduced asymmetry on a $N = 20$ -
 248 player, well-mixed population. Figure 3(a) compares the frequency of communicative
 249 strategies f_{comm} to the maximum joint benefit B_0 . The marks represent the simulation
 250 results and the lines represent the full analytic result (Eq. 10 in supplementary material)
 251 for a well-mixed population. The B_0 step size is 0.04, and the simulations ran for 2×10^8
 252 time steps. In general, f_{comm} is low for small B_0 , rises to $f_{\text{comm}} = 0.5$ at some break-even
 253 B_0 , and plateaus to $f_{\text{comm}} \approx 1$ for large B_0 . We can validate our model by comparing
 254 our $\alpha = 0.5$ case with a previous study⁶ to observe qualitatively similar results, with
 255 our break-even $B_0 \approx 0.21$ corresponding to their $B_0 = 2(N - 1)c/(N - 2) = 0.21$
 256 break-even condition. We also see that increasing (decreasing) the asymmetry α dilates
 257 (stretches) this sigmoid function in the B_0 direction. This α -dependence is reasonable,
 258 as increasing α corresponds to biasing the payoff in a mixed CN interaction towards
 259 the communicative partner.
 260
 261
 262
 263
 264
 265
 266
 267
 268
 269
 270

271 While Fig. 3(a) displays the time-averaged system state, it is also useful to inves-
 272 tigate the time-dependent variations. Figures 3(b) to 3(d) depict the frequency of
 273 communicative strategies f_{comm} as scatter plots of time on the left vertical axis for
 274 different values of the asymmetry α . These time-series points are color-coded grey if
 275
 276

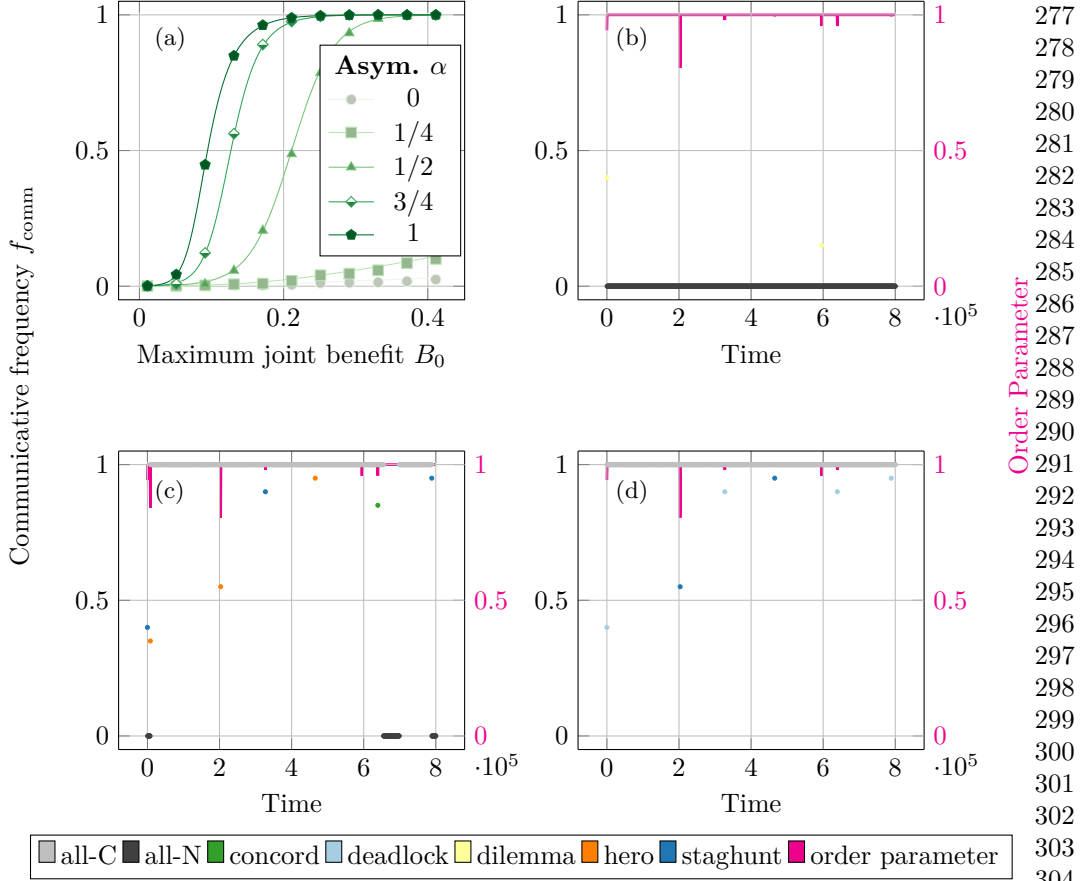


Fig. 3 | Impact of symmetry breaking on neural synchronization in well-mixed populations. Communication frequency f_{comm} for the well-mixed topology. (a) Time-averaged f_{comm} as a function of the maximum joint benefit B_0 for different values of the payoff asymmetry α . The marks represent the simulation results and the lines represent the theory predictions. (b)–(d) Scatter plots where the left vertical axes show the instantaneous f_{comm} as a function of time and are color-coded according to the plurality mixed game type as indicated in the legend. The right vertical axes give the order parameter ρ (Eq. 4), in magenta, as a function of time. The asymmetry is (b) $\alpha = 0$, (c) $\alpha = 0.75$, and (d) $\alpha = 1$.

all players are communicative or black if all players are non-communicative; otherwise, the points are colored according to the plurality mixed game type, as indicated in the legend. On the right vertical axes, magenta line plots depict the order parameter $\rho \in [0, 1]$ given by Eq. (4).

323 Figure 3(b) shows the time-variation when the system heavily favors non-
 324 communicative players with $\alpha = 0$. After an initial disordered, dilemma-type game
 325 (yellow), the system synchronizes in the non-communicative regime (black line at
 326 $f_{\text{comm}} = 0$) with only a brief dilemma-type game excursion near time step 6×10^5 .
 327
 328 Figure 3(c) depicts an asymmetry $\alpha = 0.75$ that moderately encourages communica-
 329 tiveness. The system is synchronized in a communicative state (gray line at $f_{\text{comm}} = 1$)
 330 92% of the time, with unstable excursions to synchronized, non-communicative states
 331 (black line at $f_{\text{comm}} = 0$) and disordered, hero (orange) and staghunt (dark blue) game
 332 types. This 92% communicative rate is higher than the expected 75% from Fig. 3(a)
 333 (for $B_0 = 0.15$ and $\alpha = 0.75$), likely due to the small timespan shown in Fig. 3(c).
 334
 335 Finally, Fig. 3(d) shows the $\alpha = 1$ case where communication is heavily incentivized.
 336 Like the (b) $\alpha = 0$ case, the system is virtually always synchronized in the communica-
 337 tive regime, with only brief excursions to deadlock (light blue) or staghunt (dark blue)
 338 games types. We note that all three (b)-(d) scenarios are virtually always synchronized;
 339 the order parameter ρ (magenta) is almost always $\rho = 1$, with only occasional dips.
 340
 341 The temporary drops in communicative frequency f_{comm} and order parameter ρ are
 342 likely the result of mutations which occur, on average, every $1/\mu = 1 \times 10^4$ time steps.
 343
 344
 345
 346
 347
 348
 349
 350
 351
 352
 353
 354
 355
 356
 357

358 2.4 *C. elegans* graphs

359 Here, we consider the weighted, directed hermaphroditic *C. elegans* chemical connec-
 360 tome⁷. For reference, Fig. 4(d) shows the $N = 300$ nodes and the directed edges (we
 361 exclude the two unconnected neurons CANL/CANR). The nodes are colored according
 362 to their strategy at a particular time step, with blues representing communicative
 363 strategies and reds representing non-communicative ones, and different shades cor-
 364 responding to different phases ϕ . We note the chimera-like character of the large,
 365 synchronized group of red nodes coexisting with disordered neighboring nodes.
 366
 367
 368

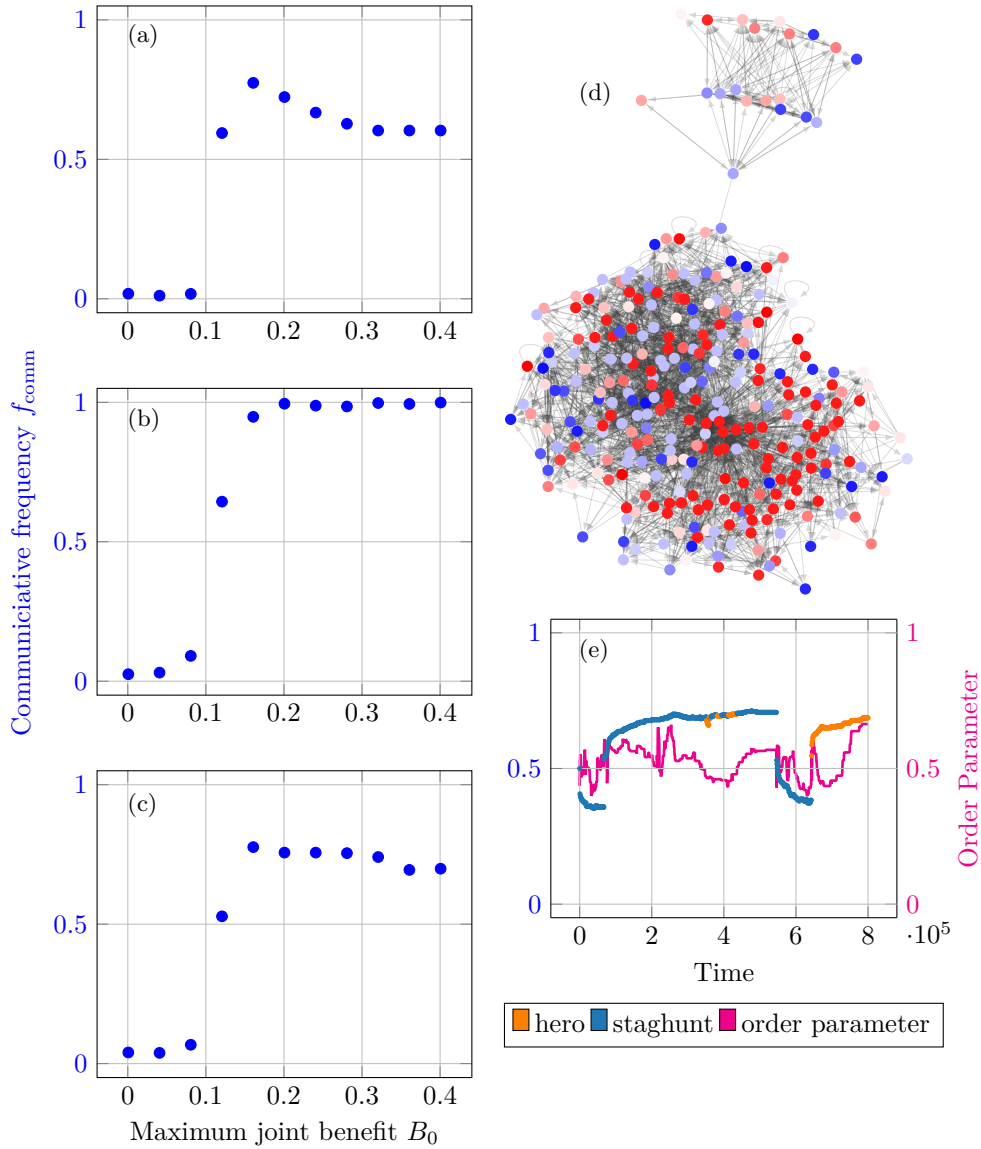


Fig. 4 | Rise of chimera states in *C. elegans* neural network. (a)–(c) Time-averaged fraction of players that are communicative as a function of the maximum joint benefit B_0 . The network topologies are the (a) weighted, directed *C. elegans* connectome, (b) unweighted, directed *C. elegans* connectome, and (c) weighted, undirected *C. elegans* connectome. (d) The network topology for the *C. elegans* $N = 300$ weighted, directed connectome with asymmetry $\alpha = 0.75$. The colors represent the $2m = 40$ strategies at a particular time step; blue colors are communicative, red colors are non-communicative, and shades represent different phases ϕ . (e) Scatter plot with the same axes and coloring as Figs. 3(b) to 3(d) showing the communicative frequency, plurality mixed game-types, and order parameter.

369
370
371
372
373
374
375
376
377
378
379
380
381
382
383
384
385
386
387
388
389
390
391
392
393
394
395
396
397
398
399
400
401
402
403
404
405
406
407
408
409
410
411
412
413
414

415 Next, to quantify the observations of Fig. 4(d), Fig. 4(a) shows the fraction of
 416 players using communicative strategies f_{comm} averaged across the entire simulation of
 417 2×10^8 time steps as a function of the maximum joint benefit B_0 in 0.04 steps for the
 418 $C. elegans$ connectome network topologies. All subplots use an asymmetry of $\alpha = 0.75$.
 419

420 We note that the behaviour of the (a) $C. elegans$ case is qualitatively distinct from
 421 the $\alpha = 0.75$ well-mixed case in Fig. 3(a). The communicative fraction f_{comm} is flatter
 422 for $B_0 \leq 0.08$, has a steep jump to 0.77 at $B_0 = 1.6$, and decreases to a horizontal
 423 asymptote around 0.60. We can isolate the cause of this deviation from the Fig. 3(a)
 424 well-mixed behavior by looking at variations to the Fig. 4(a) $C. elegans$ network
 425 topology. First, the (b) *directed*, unweighted connectome is qualitatively similar to
 426 the (a) well-mixed case with a monotonic increase from low communicativeness for
 427 $B_0 < 0.1$ to full communicativeness for $B_0 \geq 0.2$. This implies that directedness plays
 428 only a small role in the qualitative shape of the (a) full $C. elegans$ case. Conversely,
 429 the (c) *weighted*, undirected connectome looks similar to the (a) full $C. elegans$ case,
 430 displaying the same plateau at $f_{\text{comm}} \approx 0.7$, though the peak around $B_0 = 0.15$ is less
 431 pronounced. This similarity implies that the connectome’s edge weights cause most of
 432 the deviation between the (a) full $C. elegans$ case and the Fig. 3(a) well-mixed case.
 433

434 We can also investigate the time-evolution of the $C. elegans$ system using the
 435 same parameters as the Figs. 3(b) to 3(d) well-mixed case but with the $C. elegans$
 436 connectome graph. Compared to the well-mixed case, the (e) $C. elegans$ case depicts a
 437 far more heterogeneous population. Here, the population never stabilizes to a fully
 438 communicative or non-communicative state. Instead, both its communicative frequency
 439 and order parameter stay between 40 % to 70 %. The mean communicative frequency
 440 $f_{\text{comm}} \approx 60\%$ is similar to the expected $f_{\text{comm}} \approx 70\%$ from Fig. 4(a) with $B_0 = 0.15$;
 441 the discrepancy likely comes from the stochasticity in this small, 8×10^5 time-step
 442 subset. And while the Fig. 3(c) well-mixed setup displays hero, staghunt, and concord
 443 plurality mixed game-types, the Fig. 4(e) $C. elegans$ setup only displays hero and
 444
 445
 446
 447
 448
 449
 450
 451
 452
 453
 454
 455
 456
 457
 458
 459
 460

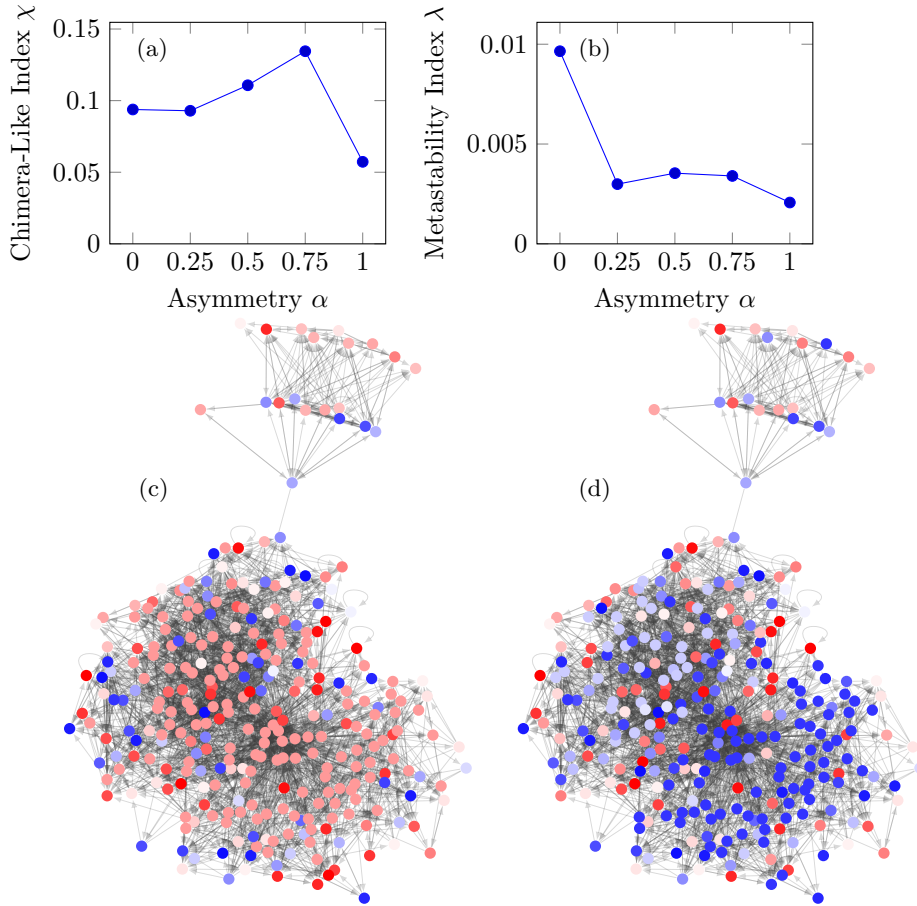


Fig. 5] Characterizing chimera states. (a) The chimera-like index (Eq. 6) and (b) metastability index (Eq. 7) as functions of the asymmetry α for the weighted, directed *C. elegans* connectome. To calculate the indices, we split the graph into two communities according to the nodes' relative covariance (*cf.*, Section 4.8). (c)–(d) A snapshot of the *C. elegans* connectome where blue colors are communicative, red colors are non-communicative, and shades represent different phases ϕ . The asymmetry is (c) $\alpha = 0$ or (d) $\alpha = 1$.

staghunt games. Finally, the *C. elegans* case is less stable to mutations than the Fig. 3(c) well-mixed case: instead of stable synchronized states with transient impulses, the *C. elegans* case depicts disordered states with discontinuous offsets.

507 2.5 Chimera-like index

508
509 Time-lapse animations of the system’s time evolution show a subset of the nodes
510 exhibiting high synchronicity with others remaining disordered: this is characteristic of
511 a chimera state. Animations depicting this phenomena are available as supplementary
512 videos, and an interactive website for exploring the full data set through plots and
513 animations is provided in the “Code availability” section at the end of the paper. In
514 order to quantify this chimera-like effect, we will investigate the chimera-like index χ
515 (Eq. 6) and metastability index λ (Eq. 7). As discussed in Section 4.8, the chimera-like
516 index measures the coherence difference between communities of players, is equal to
517 the time-averaged community covariance, and has a theoretical maximum value of
518 $M/[4(M - 1)] = 0.5^{20}$ for our $M = 2$ communities. Conversely, the metastability index
519 represents how often the system transitions between synchronicity and disorder, is equal
520 to the community-average of the temporal covariance, and has a practical maximum
521 of 0.08²⁰. Figure 5 shows the (a) chimera-like index χ and (b) metastability index λ
522 as functions of the asymmetry α . These simulations ran with the same parameters as
523 the Figs. 4(a) to 4(c) *C. elegans* time-series data.

534 The metastability displayed in Fig. 5 is less than 0.01, much smaller than the
535 practical maximum of 0.08. This implies that the system has low metastability and
536 spends most of its time at a nearly constant synchronicity $\rho_m(t)$. Furthermore, while
537 the metastability is higher (more stability variations) at $\lambda \approx 0.01$ for the $\alpha = 0$ case,
538 the metastability drops precipitously for larger α , always staying below 0.004 implying
539 that higher asymmetry α makes the system more stable. Conversely, the chimera-like
540 index χ indicates a high chimeric quality with values (0.06 to 0.13) nearly a quarter
541 of the theoretical maximum (0.5). Given that we average the chimera-like index over
542 time, the system’s deviation from a complete chimera state arises from both imperfect
543 separation of the coherent/disordered populations as well as time fluctuations in the
544 chimeric quality. While we observe that χ has a maximum at $\alpha = 0.75$, we caution
545
546
547
548
549
550
551
552

that this is likely the result of calculating the communities based on the $\alpha = 0.75$ covariances. Nevertheless, the high χ value for all asymmetries α implies that the strong chimeric character is intrinsic rather than an artifact of our $\alpha = 0.75$ choice.

2.6 Game types

Next, we seek to understand the types of games that nodes play during the population’s evolution. In Fig. 6, we investigate the plurality game type amongst all player interactions at each time step (*cf.*, Section 4.6). Figure 6 shows the fraction of time that a given game type is the plurality for different values of the asymmetry α for (a) $N = 20$ well-mixed, and (b) *C. elegans* connectome network topologies. The (a) well-mixed case fully-synchronized to all-communicative or all-noncommunicative for over 99.6% of the runtime across every asymmetry α , as corroborated by the order parameter $\rho \approx 1$ in Figs. 3(b) to 3(d). Furthermore, the α -dependence of the communicative synchronization (“all-C”) fraction approximates the communicative frequency f_{comm} in Fig. 3(a) for $B_0 = 0.15$. In contrast, the (b) *C. elegans* system is never synchronized, but instead is virtually always dominated by coordination (*CC*) and neutral (*NN*) game types.

In order to investigate the other game types involved, we can also consider the plurality *mixed* game type (*cf.*, Section 4.6). The (c) well-mixed case only changes for the $< 1\%$ of the time when unsynchronized. In order to better observe these game types, a blue inset below Fig. 6(c) magnifies these small fractions. In contrast, the (d) shows a variety of most-frequent game types that vary based on the asymmetry: dilemma for $\alpha = 0, 0.25$, chicken for $\alpha = 0.5$, hero for $\alpha = 0.75$, and deadlock for $\alpha = 1$. We note that these dominant game types are the same as the most-frequent *disordered* (*i.e.*, states other than “all-C” or “all-N”) plurality mixed games as those played in the Fig. 6(c) well-mixed setup (*cf.*, blue inset) for each α . Additionally, the *C. elegans* system displays some game-type heterogeneity, with a second game type (staghunt) being the plurality 1% to 18% of the time for asymmetries $\alpha \geq 0.5$. Overall,

599
600
601
602
603
604
605
606
607
608
609
610
611
612
613
614
615
616
617
618
619
620
621
622
623
624
625
626
627
628
629
630
631
632
633
634
635
636
637
638
639
640
641
642
643
644

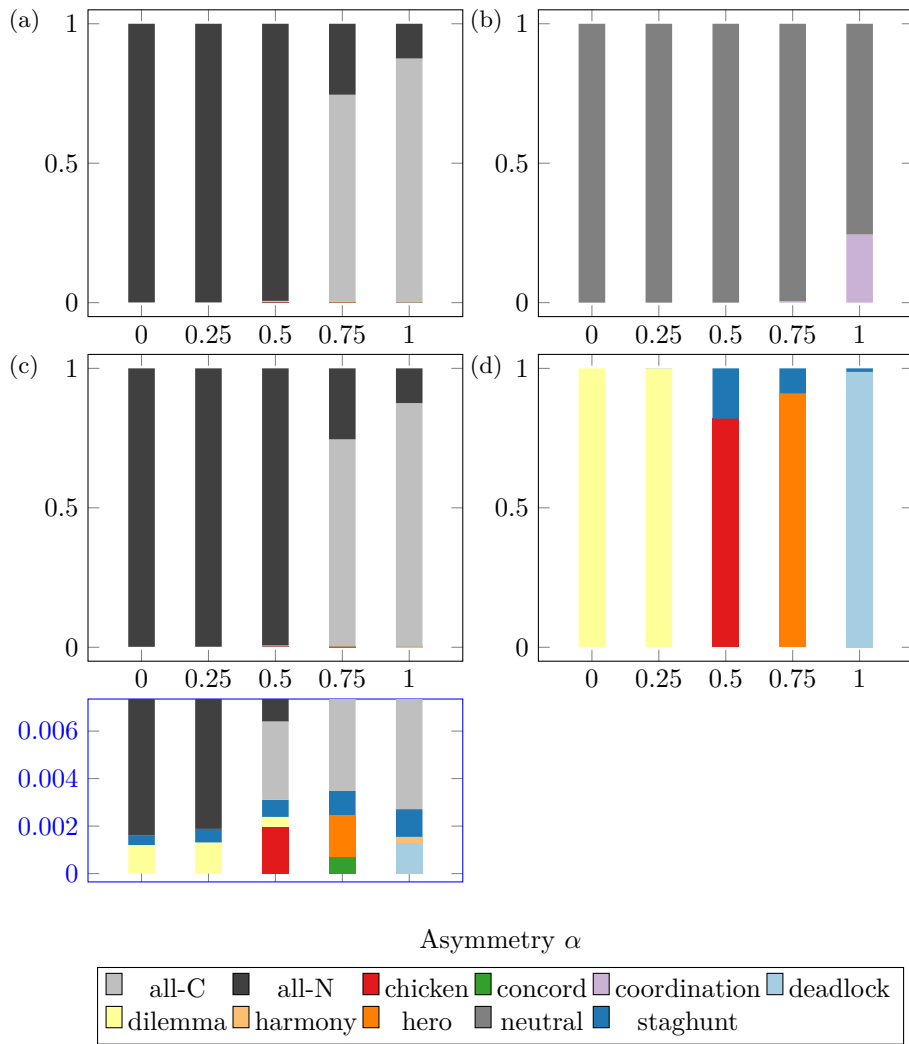


Fig. 6 | Influence of payoff asymmetry on game types played. The plurality game type amongst all player interactions expressed as a fraction of all games played for different values of the asymmetry α . The game types are color-coded according to the legend; additionally, “all-C” and “all-N” represent when the population is entirely synchronized to communicativeness or non-communicativeness, respectively. The network topologies are the (a) $N = 20$ well-mixed population and (b) weighted, directed *C. elegans* connectome. Similarly, (c), (d) depict the plurality game type when only considering mixed game types for the (c) $N = 20$ well-mixed population and (d) weighted, directed *C. elegans* connectome. A blue inset below the (c) well-mixed panel shows the magnified lower region.

we see that graph structure decreases synchronization and asymmetry influences the dominant game types, which, in turn, underpin the formation of chimera states.

3 Discussion

We can validate our Fig. 6(c) well-mixed time-series results by comparing the $\alpha = 0.5$ case to previous studies⁶. Their weak-selection $\delta = 0.2$ results also show the system spending virtually all of its time in a synchronized state. When not synchronized, their system had plurality chicken (denoted “snowdrift” therein) and staghunt (denoted “coordination”, not to be confused with the coordination-type game here) games. Indeed, Fig. 2(a) shows that staghunt, dilemma, and chicken would be the only game types accessible for $\alpha = 0.5$, which is corroborated in our simulations by the inset below Fig. 6(c).

Next, we will discuss the observed chimera states. While the chimera-like quality is inherently time-dependent (*cf.*, Eq. 6) carefully chosen snapshots can still convey some of the chimera-like aspects. Figure 5(c) shows a snapshot of the communication strategies for asymmetry $\alpha = 0$ using the same color scheme as Fig. 4(d). We notice a large region of light red representing a synchronized group of non-communicators, as well as a mix of disordered neighbors. This coexistence of strong synchronization and disorder is consistent with the high chimera-like index χ observed in Fig. 5 for $\alpha = 0$. Likewise, the $\alpha = 0.75$ case depicted in Fig. 4(d) has an even higher $\chi = 0.13$, consistent with the coexistence of a large, synchronized non-communicative group (red) and disordered neighbors (varying phases/colors). In contrast, Fig. 5(d) shows a snapshot for $\alpha = 1$, for which we expect a lower chimera-like index of $\chi = 0.06$. Indeed, we see that the large communicative (red) group in Fig. 5(d) or Fig. 4(d) has fractured into two communicative (blue) groups with different phases (color shade), lowering the chimeric quality. Therefore, these snapshots give a glimpse of the chimera-like quality in the *C. elegans* populations.

691 We also note that Fig. 6 shows that the high chimera-like index setups ($\alpha = 0.5, 0.75$)
692 are dominated by game types (chicken, hero, and battle), shown in warm colors (red,
693 orange, and pink, respectively), with exponentially slow fixation times²¹. In contrast,
694 the lower chimera-like index setup ($\alpha = 0, 0.25, 1$) is dominated by non-exponentially-
695 slow dilemma and deadlock type games. This connection between exponentially-slow
696 fixation time games and high chimera index seems suggestive and requires further
697 investigation.
700

701
702 Another study of the *C. elegans* connectome also found chimera-like states using
703 an entirely non-game-theory tool, modular neural networks⁴. That study found a
704 maximum chimera-like index of 0.12, in agreement with our value of 0.13, despite the
705 different network models of the *C. elegans* connectome considered. This agreement
706 between two different models of neurons reveals that the emergence of chimera states
707 is most likely primarily driven by the connectivity structure itself.
709

710
711 Chimera states of networked oscillators exhibit coexisting synchronized and disor-
712 dered populations, are present in brains^{1,2}, and may be pivotal in human cognition².
713 Prior studies¹⁸ investigated chimera-like brain states in *Drosophila melanogaster* (*D.*
714 *melanogaster*) using sinusoidally-coupled Kuramoto oscillators, a frequent model for
715 neuron dynamics¹⁷. However, the small-scale evolutionary factors leading to chimera-
716 like states remains poorly understood. In this paper, we extended the evolutionary
717 Kuramoto model to include weighted, structured interaction graphs and an asymmetry
718 between the communicator and non-communicator payoffs. We first applied this model
719 to a well-mixed population and found that increasing (decreasing) the asymmetry
720 inhibits (promotes) communicativity. Next, we applied the model to a family of graphs
721 deriving from the *C. elegans* connectome. This revealed that the graph's weighted-
722 ness has a much stronger influence on the communication frequency than the graph's
723 directedness does. Finally, while the well-mixed players have homogeneous populations
724 that occasionally switch between synchronized communicative and non-communicative
725
726
727
728
729
730
731
732
733
734
735
736

states, the *C. elegans* population remains far more heterogenous with a stable, chimeric mix of disordered game types.

Future work will focus on applying the EK model to families of generative brain network models²². The limited number of empirical graphs analyzed in this study hinders the identification of exact relationships between the communicative fraction and graph properties such as edge degree, weight, and directionality. However, applying the model to parameterized families of graphs could allow for fine-tuning the parameters to extract these relations. Additionally, since this study only considers a single species' connectome, it is unclear if our findings regarding the dependence of chimeric activity on graph structure are generalizable. Therefore, it is of interest to investigate this connection further by applying our EK setup to other model organisms, such as that of *Drosophila melanogaster*²³.

A key takeaway from this study was the importance of edge weight on communicativity; this has important parallels to neural computing, where edge weights are a primary driver of functionality. Additionally, the observation of chimeric states arising from such simple neurogame-theoretic models implies that the nature of neuron interactions is likely a key component in producing these critical brain states. Overall, evolutionary graph theory allowed us to connect low-level payoff details for individual neurons to high-level phenomena such as chimera-states, and this model could serve as a valuable computational framework for clarifying the influence of network structure on neural dynamics.

4 Methods

4.1 Game setup

We model the system of evolving, coupled oscillators by discretizing the 2π phase angle into m discrete phases $2\pi j/m$ for $j \in 0, \dots, m - 1$. The game's strategy space is the outer product of the m phases ($m = 20$ for our simulations) and 2 communicative

783 choices, communicative C and non-communicative N . For a given pair of phases, ϕ_i
784 and ϕ_j , the game is specified by the payoff matrix. If one player is communicative and
785 the other is non-communicative (“mixed game”, CN or NC), the payoff matrix is
786
787

$$788$$

$$789$$

$$790 \begin{array}{cc} & C, \phi_i & N, \phi_j \\ \begin{array}{c} C, \phi_i \\ N, \phi_j \end{array} & \left[\begin{array}{c|c} B_0 f(0) - c & 2\alpha\beta_0 f(\Delta\phi) - c \\ \hline 2(1-\alpha)\beta_0 f(\Delta\phi) & 0 \end{array} \right] & \end{array}, \quad (1)$$

$$791$$

$$792$$

$$793$$

$$794$$

$$795$$

796 if both players are communicative (CC), the matrix is
797

$$798$$

$$799$$

$$800 \begin{array}{cc} & C, \phi_i & C, \phi_j \\ \begin{array}{c} C, \phi_i \\ C, \phi_j \end{array} & \left[\begin{array}{c|c} B_0 f(0) - c & B_0 f(\Delta\phi) - c \\ \hline B_0 f(\Delta\phi) - c & B_0 f(0) - c \end{array} \right] & \end{array}, \quad (2)$$

$$801$$

$$802$$

$$803$$

$$804$$

$$805$$

806 and if both are non-communicative (NN), the matrix is
807

$$808$$

$$809$$

$$810 \begin{array}{cc} & N, \phi_i & N, \phi_j \\ \begin{array}{c} N, \phi_i \\ N, \phi_j \end{array} & \left[\begin{array}{c|c} 0 & 0 \\ \hline 0 & 0 \end{array} \right] & \end{array}, \quad (3)$$

$$811$$

$$812$$

$$813$$

$$814$$

$$815$$

816 with $f(\Delta\phi) = [1 + \cos(\phi_j - \phi_i)]/2$ (Fig. 1(c)). Here, B_0 , β_0 , α , and c are fixed parameters
817 defining the game. The cost c represents the penalty paid by communicative players,
818 and B_0 and β_0 are the maximum benefits paid with joint CC communicators and
819 mixed CN players, respectively. The phase-dependent function $f(\Delta\phi)$ encodes the
820 influence of phase mismatches. Finally, the benefit asymmetry $\alpha \in [0, 1]$ breaks the
821 symmetry between the payoff for the communicator and the non-communicator when
822 exactly one player is communicative.
823
824
825
826
827
828

4.2 Population setup	829
	830
Given N players, we associate a pair of weighted, directed graphs to the population.	831
First, we use an interaction graph with N nodes representing players and weighted,	832
directed edges representing games between players. Second, we implement a reproduc-	833
tion graph with the N nodes still representing players but the edges now corresponding	834
to the ability of nodes to replace one another. For simplicity, our reproduction graphs	835
are identical to the interaction graph with a single self-loop added to each node. These	836
self-loops are necessary in the reproduction graph to ensure that each node has positive	837
indegree as required by the Moran process described in the next section.	838
	839
	840
	841
	842
	843
	844
	845
	846
4.3 Birth-death Moran process	847
	848
The population is updated according to a birth-death Moran process with exponential	849
fitness ²⁴ . On each turn, the following steps are performed. First, each edge in the	850
interaction graph corresponds to a game between head node i and tail node j , the	851
edge's payoff π_{ji} is scaled by the edge weight w_{ji} , and the relevant payoff $w_{ji}\pi_{ji}$ is	852
awarded to the head node only. Since the <i>C. elegans</i> edge weights are integers, we can	853
also interpret each edge weight as the number of games played between the two nodes.	854
Figure 1(b) shows an illustration of this process for a single pair of interacting players	855
connected by a pair of weighted, directed edges. The total fitness for node i is the	856
exponential of the product between the selection strength δ and the sum of payoffs to	857
node i , or $f_i = \exp(\delta \sum_j w_{ji}\pi_{ji})$ with the sum over all edges inwardly incident to node	858
i . Then, a single focal node is chosen for reproduction with probability proportional	859
to the node's fitness f_i . Finally, a node is chosen for replacement amongst the birth	860
node's out-neighbors with probability proportional to the reproduction graph's edge	861
weight. With mutation probability μ , the death node is replaced by a player with a	862
uniformly random strategy; otherwise, it is replaced by a player with the same strategy	863
as the birth node. This birth-death process is repeated for each turn.	864
	865
	866
	867
	868
	869
	870
	871
	872
	873
	874

875 4.4 Communication frequency

876

877 We define the frequency of communicative strategies $f_{\text{comm}}(t)$ as the fraction of

878

879 players employing a communicative strategy C at a given time step. We also define

880

881 the time-averaged communicative frequency f_{comm} by averaging $f_{\text{comm}}(t)$ over the

882

882 entire simulation. For simulation times long compared to the mutation turnover time

883

884 $T_{\text{turn}} \gg N/\mu$, the initial, random distribution of strategies will be negligible and the

885

886 time-average will correspond to the long-time limit. In section 2 of the supplementary

887

887 material, we derive an analytic expression (Eq. 10 of supplementary materials) for

888

889 f_{comm} in the well-mixed case by incorporating the benefit asymmetry α .

890

891

892

893 4.5 Game type nomenclature

894

895 Every edge of the interaction graph defines a game between the two players it connects.

896

897 Using their relative phase difference $\Delta\phi$, we can calculate the payoff matrix. By

898

898 comparing the order of each of the four entries, we determine the game type using a

899

900 topological taxonomy¹⁹. Using this taxonomy, we calculate the ordinal rank of the

901

902 four entries in the Eq. (1) payoff matrix and assign a unique name (*e.g.*, dilemma,

903

903 deadlock, chicken, *etc.*) to each strict, symmetric game type. However, Fig. 2(b) shows

904

905 that some mixed CN games lie on the border between two game types, such as when

906

906 $\alpha = 1$ or $B/c = 0$ (bordering game types for $B/c > 0$ and $B/c < 0$, not shown).

907

908 The taxonomy¹⁹ classifies these non-strict games according the number and location

909

910 of ties (“high tie”, “middle tie”, “double tie”, *etc.*). It also defines a convention for

911

912 choosing one of the neighboring game types to get a binomial nomenclature (*e.g.*,

913

913 “high harmony”, “mid compromise”, “double coordination”, *etc.*). We follow the same

914

915 convention for choosing a neighboring game but drop the tie-indicator to keep our

916

916 figure legends simple. Specifically, referring to Fig. 2(b), the $\alpha = 1$ tie between deadlock

917

918 and compromise games formally corresponds to “low [dead]lock”, but we label it as

919

919 deadlock; similarly, the tie between assurance and staghunt is “mid staghunt”, but

920

we denote it as staghunt. Likewise, all of the $B/c = 0$ payoff matrices correspond to the “double harmony” game type, but we denote them as simply “harmony”. Finally, the NN game type is always “neutral” while the CC game type is always “double cooperation”, which we denote as just “cooperation”.

4.6 Plurality game type

At each time step, we calculate the game type for each edge of the interaction graph. We determine the game type by creating a two-by-two payoff matrix of possibilities where both players have the hypothetical option of switching to the other player’s strategy/phase pairing. Using the taxonomy discussed in Section 4.5, we then assign a game type to that interaction. We then identify the plurality game type across all player interactions, where each edge’s count is weighted by its edge weight. Then, we calculate the frequency of this “plurality game” across all time steps of a given simulation to determine the distribution of games commonly played. This “plurality game-type” metric, as depicted in Fig. 6(a) and Fig. 6(a), is often dominated by neutral games (between NN players) and coordination games (between CC) players. To isolate the other game types involved, we also defined a “plurality *mixed* game-type” by only counting games between mixed CN or NC pairs in the plurality (or labelling the time step as “all-communicative”/“all-noncommunicative”, as necessary). This “plurality mixed game-type” shows more variety and is depicted in all of the other figures (Fig. 3, Fig. 4, Fig. 6(c) and Fig. 6(c)). Note that an edge’s game type is dependent on the players’ dynamically-evolving communication strategies (N or C) and relative phase $\Delta\phi$, as well as the fixed game parameters c , B_0 , β_0 , and α . Furthermore, this metric is only sensitive to the plurality game and therefore provides no information on the presence/absence of minority game types.

967 4.7 Order parameter

968

969 Given that the Kuramoto system of coupled oscillators inspired this evolutionary game

970

971 model, we also define the standard Kuramoto order parameter:

972

973

974

975

976

977

$$\rho = \frac{1}{N} \left| \sum_{j=1}^N e^{i\phi_j} \right| \quad (4)$$

978 This parameter ranges from zero to one, inclusive, and represents how coherent the

979

980 population is, with $\rho = 1$ for fully coherent and $\rho = 0$ fully disordered.

981

982

983 4.8 Chimera-like index and metastability index

984

985 To compare with a previous analysis⁴ of chimera-like states *C. elegans* models, we

986

987 define a pair of indices related to chimera-like quality and metastability²⁰. First, we

988

989 organize the game's nodes into M disjoint communities. We split the nodes into $M = 2$

990

991 communities C_m by taking a subset (the first 8×10^4 steps for computations ease)

992

993 of the simulation results for the *C. elegans* simulation with asymmetry $\alpha = 0.75$.

994

995 We then calculate the covariance matrix $K_{i,j}$ of the strategy indices, ensuring that

996

997 communicative (C, ϕ_i) and non-communicative (N, ϕ_i) are treated distinctly. Next, we

998

999 calculate the row-wise covariance-sums $\sum_i K_{i,j}$ and form a community by collecting

1000

1001 all nodes j with covariance-sum at least 1,500, *i.e.*, $\sum_i K_{i,j} \geq 1500$. Note that 1,500 is

1002

1003 chosen as a high cutoff to ensure we only group nodes with high covariance-sum; for

1004

1005 reference, 1,500 is approximately 81 % of the maximum covariance-sum. Finally, we

1006

1007 place all the remaining nodes in a second community.

1008

1009 With these disjoint communities C_m , we then calculate the time-dependent,

1010

1011 community-wise order parameter $\rho_m(t)$ as

1012

$$\rho_m(t) := \frac{1}{N_m} \left| \sum_{j \in C_m} e^{i\phi_j} \right| \quad (5)$$

across members j of community C_m with size N_m . Then, we define a chimera-like index χ

$$\chi = \langle \sigma_{\text{chi}} \rangle_T \quad (6)$$

where

$$\sigma_{\text{chi}} := \frac{1}{M-1} \sum_{m=1}^M \left(\rho_m(t) - \langle \rho_m(t) \rangle_M \right)^2$$

and a metastability index λ

$$\lambda = \langle \sigma_{\text{met}} \rangle_M \quad (7)$$

where

$$\sigma_{\text{met}} := \frac{1}{T-1} \sum_{t=1}^T \left(\rho_m(t) - \langle \rho_m(t) \rangle_T \right)^2$$

across the M communities and T time steps. The chimera-like index measures the difference in coherence between communities: complete homogeneity between communities (*e.g.*, all fully synchronized *or* fully disordered) corresponds to $\chi = 0$, while having M communities with half fully synchronized ($\rho_m = 1$) and the other half fully disordered ($\rho_m = 0$) for all times yields a maximum $\chi = M/[4(M-1)] = 1/2$ for our $M = 2$ ²⁰. Likewise, the metastability index λ measures how metastable the system is (*i.e.*, transiting between synchronicity and disorder). A system that is fully synchronized or disordered gives $\lambda = 0$; λ is maximized for a system spending equal times in each state, where the variance of the uniform distribution gives $\lambda = 1/12 \approx 0.08$ ²⁰.

Supplementary information. Supplementary Figure 1 of two-player game order graphs. Section 1, two-player game order graphs; Section 2, derivation of well-mixed communicative fraction with symmetry breaking. Supplementary videos 1-3, time-evolution of *C. elegans* player strategies using the same color scheme as Fig. 4(d) with $B_0/c = 1.5$, $\beta_0/B_0 = 0.95$, $c = 0.1$, $\mu = 0.0001$, $m = 20$, $\delta = 0.2$, and 8×10^6 time steps; supplementary video 1 shows $\alpha = 0$, supplementary video 2 shows $\alpha = 0.75$, and supplementary video 3 shows $\alpha = 1$.

Declarations. The authors declare no competing interests.

1059 **Code availability.** An interactive webpage for exploring the data set is available at
1060 https://tzdyrski.github.io/egt-kuramoto/notebooks/EKT_Plots.html. Additionally,
1061 all source code is available via GitHub at <https://github.com/TZdyrski/egt-kuramoto/>
1062 [tree/1.0.0](https://github.com/TZdyrski/egt-kuramoto/tree/1.0.0).
1063
1064
1065
1066

1067 **Data availability.** The processed data for all simulated parameter ranges is available
1068 on Zenodo at <https://doi.org/10.5281/zenodo.17135745>.
1069
1070
1071
1072

1073 References

- 1074
1075 [1] Santos, M. *et al.* Chimera-like states in a neuronal network model of the cat brain.
1076 *Chaos, Solitons & Fractals* **101**, 86–91 (2017).
1077
1078 [2] Bansal, K. *et al.* Cognitive chimera states in human brain networks. *Science*
1079 *advances* **5**, eaau8535 (2019).
1080
1081 [3] Majhi, S., Bera, B. K., Ghosh, D. & Perc, M. Chimera states in neuronal networks:
1082 A review. *Physics of life reviews* **28**, 100–121 (2019).
1083
1084 [4] Hizanidis, J., Kouvaris, N. E., Zamora-López, G., Díaz-Guilera, A. & Antonopou-
1085 los, C. G. Chimera-like states in modular neural networks. *Scientific reports* **6**,
1086 19845 (2016).
1087
1088 [5] Abrams, D. M. & Strogatz, S. H. Chimera states for coupled oscillators. *Physical*
1089 *review letters* **93**, 174102 (2004).
1090
1091 [6] Tripp, E. A., Fu, F. & Pauls, S. D. Evolutionary kuramoto dynamics. *Proceedings*
1092 *of the Royal Society B* **289**, 20220999 (2022).
1093
1094 [7] Cook, S. J. *et al.* Whole-animal connectomes of both caenorhabditis elegans sexes.
1095 *Nature* **571**, 63–71 (2019).
1096
1097
1098
1099
1100
1101
1102
1103
1104

- [8] Towlson, E. K., Vértés, P. E., Ahnert, S. E., Schafer, W. R. & Bullmore, E. T. The rich club of the *c. elegans* neuronal connectome. *Journal of Neuroscience* **33**, 6380–6387 (2013).
- [9] Yan, G. *et al.* Network control principles predict neuron function in the *caenorhabditis elegans* connectome. *Nature* **550**, 519–523 (2017).
- [10] Sigmund, K. & Nowak, M. A. Evolutionary game theory. *Current Biology* **9**, R503–R505 (1999).
- [11] Traulsen, A. & Glynatsi, N. E. The future of theoretical evolutionary game theory. *Philosophical Transactions of the Royal Society B* **378**, 20210508 (2023).
- [12] Cohen, Y. & Cohen, J. Evolutionary game theory and the evolution of neuron populations, ring rates, and decisionmaking. *Nature Precedings* 1–1 (2009).
- [13] Antonioni, A. & Cardillo, A. Coevolution of synchronization and cooperation in costly networked interactions. *Physical review letters* **118**, 238301 (2017).
- [14] Ohtsuki, H., Hauert, C., Lieberman, E. & Nowak, M. A. A simple rule for the evolution of cooperation on graphs and social networks. *Nature* **441**, 502–505 (2006).
- [15] Su, Q., Allen, B. & Plotkin, J. B. Evolution of cooperation with asymmetric social interactions. *Proceedings of the National Academy of Sciences* **119**, e2113468118 (2022).
- [16] Bhaumik, J. & Masuda, N. Constant-selection evolutionary dynamics on weighted networks. *Proceedings of the Royal Society A* **480**, 20240223 (2024).
- [17] Cabral, J., Hugues, E., Sporns, O. & Deco, G. Role of local network oscillations in resting-state functional connectivity. *Neuroimage* **57**, 130–139 (2011).

- 1151 [18] Deng, S. & Ódor, G. Chimera-like states in neural networks and power systems.
1152
1153 *Chaos: An Interdisciplinary Journal of Nonlinear Science* **34** (2024).
1154
- 1155 [19] Bruns, B. R. Names for games: locating 2×2 games. *Games* **6**, 495–520 (2015).
1156
- 1157 [20] Shanahan, M. Metastable chimera states in community-structured oscillator
1158 networks. *Chaos: An Interdisciplinary Journal of Nonlinear Science* **20** (2010).
1159
1160
- 1161 [21] Antal, T. & Scheuring, I. Fixation of strategies for an evolutionary game in finite
1162 populations. *Bulletin of mathematical biology* **68**, 1923–1944 (2006).
1163
1164
1165
- 1166 [22] Betzel, R. F. *et al.* Generative models of the human connectome. *Neuroimage*
1167 **124**, 1054–1064 (2016).
1168
1169
- 1170 [23] Schlegel, P. *et al.* Whole-brain annotation and multi-connectome cell typing of
1171 drosophila. *Nature* **634**, 139–152 (2024).
1172
1173
- 1174 [24] Lieberman, E., Hauert, C. & Nowak, M. A. Evolutionary dynamics on graphs.
1175 *Nature* **433**, 312–316 (2005).
1176
1177
1178
1179
1180
1181
1182
1183
1184
1185
1186
1187
1188
1189
1190
1191
1192
1193
1194
1195
1196